

Radiative Cooling Smart Textiles with Integrated Sensing for Adaptive Thermoregulation

Yoon Young Choi, Kai Zhou, Ho Kun Woo, Diya Patel, Md Salauddin, and Lili Cai*

Cite This: *ACS Materials Lett.* 2024, 6, 4624–4631

Read Online

ACCESS |



Metrics & More

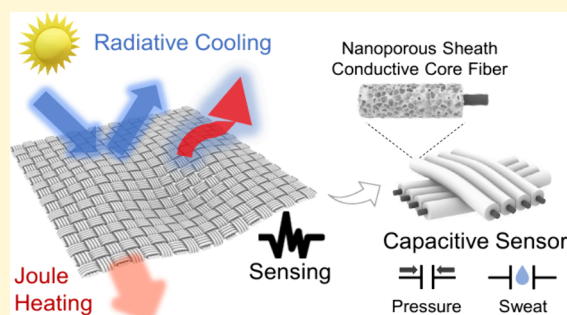


Article Recommendations



Supporting Information

ABSTRACT: Efficient and adaptive thermoregulation of smart wearable technologies could revolutionize the mitigation of health- and energy-related challenges posed by climate change. We developed a woven, thermally adaptive smart textile (TAST) with high solar reflectance and selective infrared emittance and transmittance using a scalable coaxial extrusion method to continuously manufacture core-sheath fibers. TAST enables passive outdoor radiative cooling by 6–10 °C compared to normal fabrics while preserving good mechanical strength, breathability, and washability. Due to the integration of capacitive sensing, radiative cooling, and Joule heating into the woven fibers, TAST can detect the physiological signals of the human body and adapt its thermoregulation function in response to changes in the ambient temperature and perspiration level. The superior intelligence and multifunctional performance of TAST represent a paradigm shift beyond current personal thermal management technologies for enhancing human health, wellness, and performance.



Increasingly erratic and capricious weather in recent years has presented a great challenge for personal health, as it entails drastic temperature fluctuations that are difficult to cope with.^{1–3} Many human diseases are linked to an impaired ability to adjust to rises in temperature, which can cause a dangerous increase in body temperature.^{4–8} Therefore, in the face of escalating health risks posed by climate change, there is an urgent need to advance research in personalized health monitoring and thermal management technologies.

Smart wearable technologies, along with advances in artificial intelligence (AI) and the Internet of things (IoT), have the potential to make a profound impact on our daily lives. They can enable a range of applications to improve personal health and performance, such as personalized healthcare, soft robotics, electronic skin, and human–machine interface.^{9–15} However, previous development of smart wearables tends to focus on sensing and monitoring the biosignals of the human body. Existing wearable technologies lack the requisite function for personal thermal management under different temperature conditions. Moreover, many of the previously reported wearable thermoregulation devices, such as thermoelectrics, electrochromics, and phase change materials, have several disadvantages such as bulky and heavy configurations, poor breathability, and difficulties in scalable manufacturing.^{16–20}

Passive radiative cooling and heating, on the other hand, has recently emerged as a new strategy to personal thermal management that does not require any energy cost.^{21–34} This approach utilizes the selective control of radiative heat transfer by tailoring the nano- and microscale structure of materials to achieve a cooling or heating effect.^{35–37} For example, using nanoengineered polymeric textile materials that have high solar reflectance and high infrared transmittance/emittance, radiative cooling effects of up to 2.3 and 10 °C for the human body were attained in indoor and outdoor environments, respectively.^{23–28} In the case of radiative heating, it has been shown that nanostructured metallic coatings and MXene materials can passively warm up the human body up to 7.1 °C, due to their low infrared emissivity which blocks thermal radiation dissipation to the surrounding environment.^{29–32} More recently, modulating the visible transmittance and/or infrared emissivity has been shown to enable adaptive thermoregulation using phase change materials, electrochemical tuning, and

Received: August 8, 2024

Revised: August 29, 2024

Accepted: August 30, 2024

Published: September 5, 2024



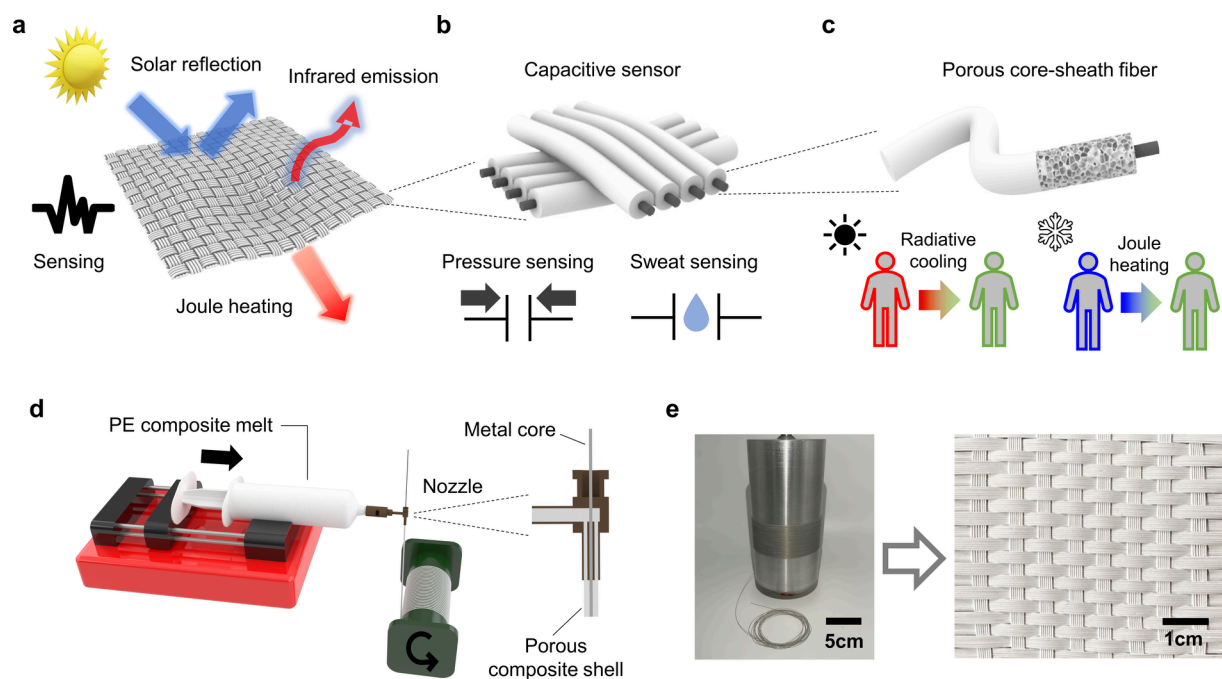


Figure 1. TAST, which is capable of radiative cooling, adaptive thermoregulation, and sensing with fabrication details. Illustration of (a) TAST with sensing capability and adaptive thermoregulation (solar reflection, infrared emission, and Joule heating); (b) the junction of warp and weft in TAST as a capacitive sensor for sensing pressure and sweat; and (c) a porous core–sheath fiber capable of radiative cooling and Joule heating. (d) Schematic of the core–sheath fiber fabrication process. (e) Photographic images of the core–sheath fibers wound around a cylinder and a TAST sample woven with the fibers.

surface wetting methods.^{38–43} Although promising progress has been made, previously reported adaptive radiative cooling/heating materials were not made in fiber form, making them unsuitable for wearable applications. Besides, they lack the ability to quickly detect the physiological status of wearers for dynamic and smart control of thermal comfort.

To address the ongoing demand for heating and cooling textiles, we developed a thermally adaptive smart textile (TAST) that incorporates passive radiative cooling structures into smart wearables with seamlessly integrated sensing capabilities at the fiber level to enable intelligent, efficient, and adaptive thermoregulation. We achieve TAST using a coaxial extrusion method to create hierarchically structured core–sheath fibers comprised of a conductive metal core and a porous polymer composite sheath. Woven from these core–sheath fibers, TAST forms a network of capacitive sensors that can detect the spatial distribution of pressure or perspiration on the textile. TAST also exhibits passive radiative cooling and active Joule heating effects due to the spectrally selective sheath and conductive core of fibers, respectively. We further demonstrate the adaptive thermoregulation capability of TAST to maintain skin temperature within the thermal comfort range of the human body under various conditions by integrating its radiative cooling, Joule heating, and capacitive sensing functions using a closed-loop feedback control system. We envision that TAST will have a significant impact on the development of smart wearable thermoregulation technologies to improve human health and societal well-being.

The design and working principles of TAST are illustrated in Figures 1a–c. TAST is a woven fabric constructed from two sets of fiber threads, i.e., warp and weft, which interlace with each other perpendicularly (Figure 1a). Each fiber consists of a porous polymer composite sheath and a conductive metal core (Figure 1c). The air pores in the sheath are engineered to be

comparable in size to the wavelengths of sunlight, resulting in strong solar reflection due to the Mie scattering effect.^{24,44–46} SiO₂ particle fillers are embedded in the polymer sheath, which can selectively emit thermal radiation in the wavelength range of 8–13 μm .^{47–50} Due to the high solar reflectance and infrared emittance/transmittance of the polymer sheath layer, TAST can achieve passive radiative cooling without any energy input. In addition, the conductive metal core of the fibers can provide Joule heating when an electrical voltage is applied. The ability to perform both cooling and heating functions is essential for the realization of adaptive thermal control. For example, under hot and intense sunlight conditions, the radiative cooling effect of TAST relieves heat stress, while Joule heating warms up the human body under cold weather conditions. Moreover, at the intersection of warp and weft, a capacitor unit is formed between the top and bottom metal fiber cores. The cores are separated by the polymer composite sheath layers as dielectrics (Figure 1b). Thus, TAST is comprised of a network of capacitive sensors, which can be utilized to detect the presence and location of stimuli that induce changes in capacitance. The fully integrated multifunctional fibers of TAST will enable the intelligent capabilities of not only tracking the status of the human body but also the utilization of sensing signals as feedback control to achieve precise, autonomous, and adaptive thermoregulation.

We experimentally fabricated TAST using a coaxial extrusion method to create hierarchically structured, multicomponent materials that are integrated at the microscale fiber level. Figure 1d shows a schematic of the fabrication procedure. In our study of model materials for TAST, we employed stainless steel wires (diameter of 100–200 μm) as the fiber core and polyethylene (PE) as the polymer matrix of the sheath coating. To attain the spectral properties for radiative cooling, PE was melted and mixed with mineral oil and SiO₂ particle fillers to

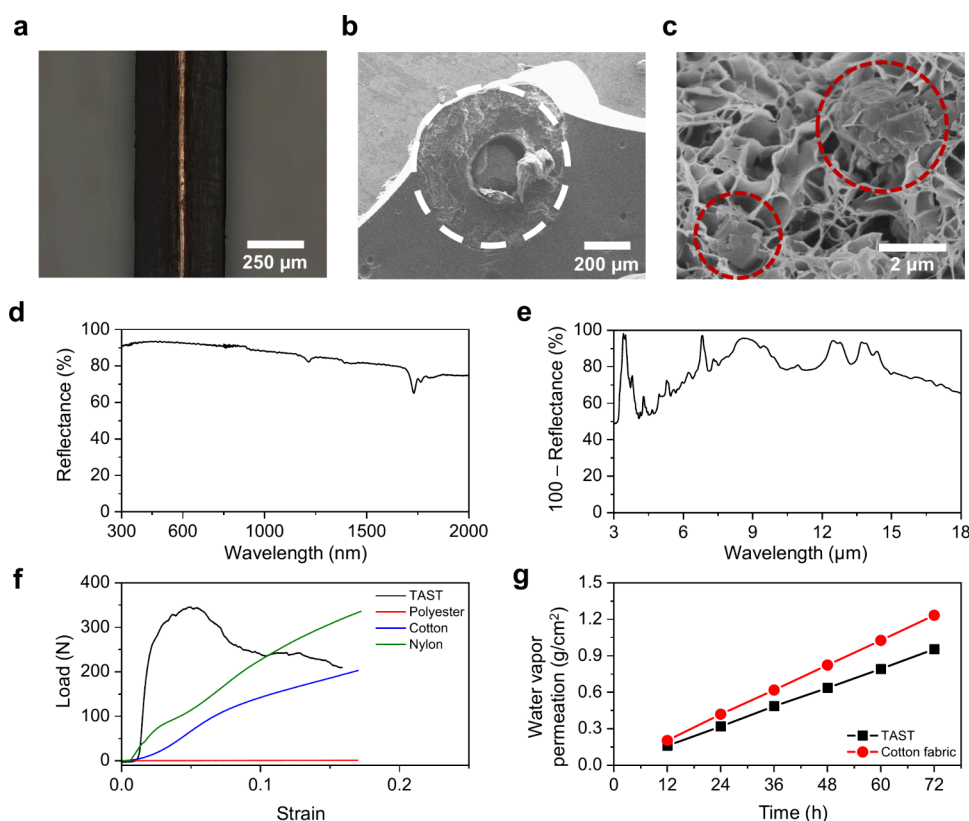


Figure 2. Properties of the core–sheath fiber and TAST. (a) Optical microscopic image of the core–sheath fiber cross-section along the longitudinal direction. (b) SEM image of the core–sheath fiber cross-section along the radial direction and (c) zoomed-in view of the porous sheath region. Characterization of (d) solar reflectance and (e) $100 (\%) - \text{reflectance} = \text{emissivity} + \text{transmittance}$ in the mid-infrared wavelength region of TAST. (f) Comparison of tensile strength for TAST, polyester, cotton, and nylon fabrics. All samples are woven fabrics. (g) Comparison of breathability for TAST and cotton (relative humidity: 40%).

form a composite. The composite melt was then heated and extruded along with the metal core wires through a coaxial needle. The coaxially extruded fibers were collected by using a rotating roller (Figure S1), allowing for continuous, scalable fabrication. By controlling the roller speed, a uniform sheath layer, with a thickness of 100–200 μm, that coats the metal wire at the core could be achieved. When the fibers were cooled after extrusion, the sheath layer solidified, containing a PE-rich phase and an oil-rich phase due to thermally induced phase separation.^{51,52} The oil phase was then extracted with a solvent, leading to the formation of an interconnected porous PE matrix with embedded SiO₂ particles. Finally, TAST was fabricated by weaving the core–sheath fibers together, with each weft and warp consisting of seven threads that were compactly placed in parallel. Figure 1e displays a roll of the extruded core–sheath fibers before oil extraction as well as the resulting woven TAST sample after oil extraction, which is opaque and white in color, indicating diffuse reflection of light. It is worth noting that the coaxial extrusion method and weaving technique for TAST production can be extended to incorporate other low-modulus electrically conductive wires, thus enhancing wearability. This versatility is illustrated by the photograph of TAST constructed with a carbon fiber core and PE sheath (Figure S2).

Figure 2a displays a top-view optical microscope photograph of a coaxially extruded fiber before oil extraction, illustrating its core–sheath construction, which comprises an inner metal wire with a diameter of 100 μm and an outer composite shell with a uniform thickness of around 200 μm. The cross-section

of the fiber along the radial direction after oil extraction was further examined by scanning electron microscopy (SEM), as shown in Figure 2b. Figure 2c exhibits a zoomed-in view of the sheath layer, confirming the formation of a porous structure with randomly distributed pore sizes of less than 2 μm. In addition, it was shown that SiO₂ particles (diameter <10 μm) were well dispersed in the porous PE matrix. Figure 2d shows that TAST made with oil/PE and SiO₂/PE mixing ratios of 7:1 (v/w) and 1:5 (w/w), respectively, achieved a high solar reflectance of 90.2% (normalized over the solar spectrum from 300–2000 nm). Additionally, this formulation exhibited an average emissivity + transmittance value of 86% within the 8–13 μm range and approached 91% around the wavelength of 9.5 μm, which is where the thermal radiation from the human body reaches its peak intensity (Figure 2e). The results for different oil/PE and SiO₂/PE ratios are shown in Figures S3–S5. The optimized oil/PE ratio for maximum solar reflectance was found to be around 7:1 or 8:1 (v/w) (Figure S3). It was also observed that the inclusion of SiO₂ had an insignificant effect on the overall solar reflectance of TAST (Figure S4), while substantially increasing the emissivity in the infrared wavelength region of 8–13 μm (Figure S5a). It is important to mention that in addition to emissivity, infrared transmittance should also be considered to evaluate the passive radiative cooling performance of textiles, given that human skin is a strong infrared emitter. It was previously shown that infrared-transparent textiles can effectively transmit the thermal radiation emitted from human skin to the surrounding environment, thereby achieving an enhanced cooling

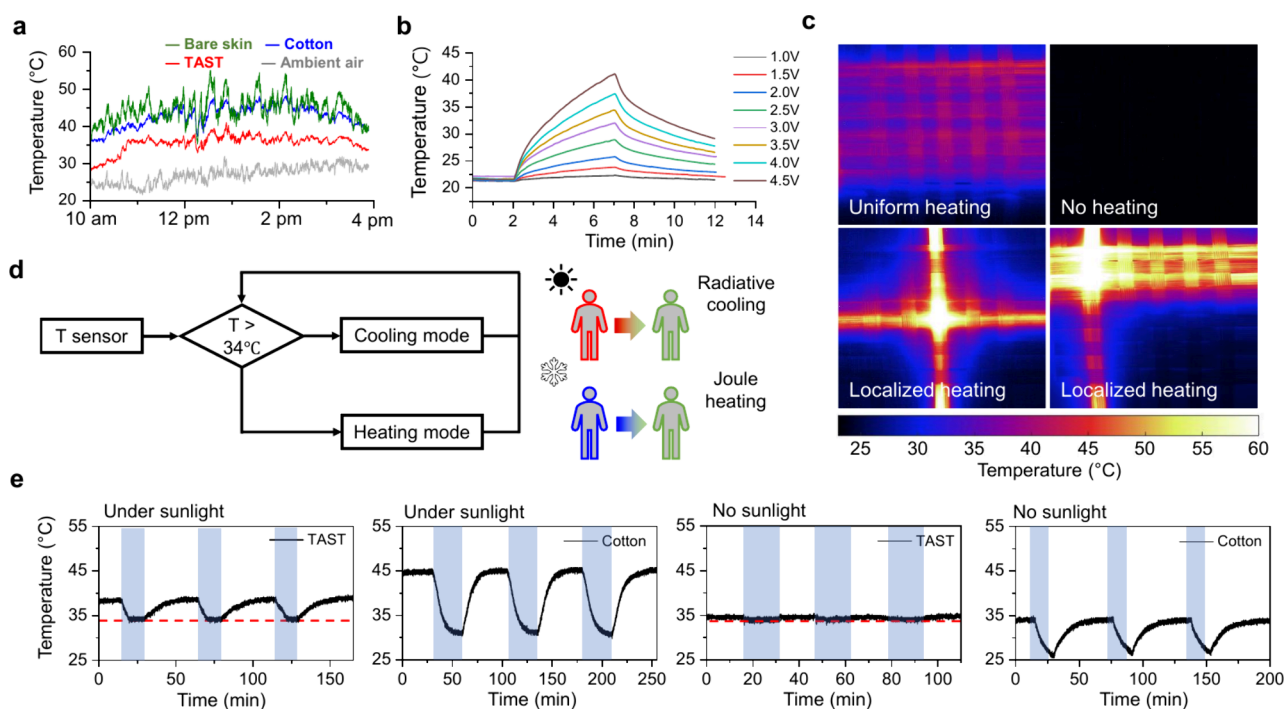


Figure 3. Radiative cooling and Joule heating performance for adaptive thermoregulation. (a) Outdoor radiative cooling test for TAST-covered (1 mm thick), cotton-covered (0.5 mm thick), and uncovered skin simulators. (b) Joule heating performance of TAST using a single fiber thread under different applied voltages. (c) Infrared thermal images of locally heated TAST. (d) Flow diagram of the closed-loop control system for adaptive thermoregulation. (e) Demonstration of the adaptive thermoregulation function for TAST in comparison to cotton fabric under sunlight (left two panels) and in the absence of sunlight (right two panels). Blue shading indicates placement of icepacks nearby.

effect.^{27,53} The 100 (%) – reflectance values, which account for both emissivity and transmittance in the infrared range, are plotted in Figure S5b for different SiO₂/PE ratios. It was found that a SiO₂/PE ratio larger than 1:5 provided the optimal emissivity + transmittance values for overall radiative cooling effects.

The mechanical strength, washability, and breathability of TAST were also evaluated. Figure 2f compares the mechanical properties of TAST with those of traditional fabrics through tensile tests, with the stress–strain curves of a single core–sheath fiber and traditional yarns shown in Figure S6. Each tensile test sample was 6 cm in width and length. Due to the high strength of stainless steel wires, TAST showed a high Young’s modulus with a maximum load of 350 N at a tensile strain of 0.05 in comparison to fabrics such as cotton, polyester, and nylon. Washing tests were conducted by stirring each sample in detergent-diluted water at 500 rpm for 30 min. The solar reflectance and infrared emissivity of TAST before and after the washing tests showed negligible differences, suggesting good durability of TAST against washing (Figure S7). Additionally, Figure S8 demonstrates the water contact angle of TAST at 125°, revealing its hydrophobic nature. This surface characteristic could be useful for attaining a self-cleaning function to mitigate the need for frequent washing. Moreover, the breathability evaluation in Figure 2g shows that TAST has a water vapor permeation rate of 13 mg/cm²·h at 34 °C, which is comparable to that of woven cotton fabrics (17 mg/cm²·h).

The thermoregulation functions of TAST were tested under various conditions. The radiative cooling performance of TAST was tested outdoors using a custom-built apparatus that simulated the thermal response of human skin, as shown in

Figure S9 (see the Experimental Methods for details). The outdoor cooling test was conducted under direct sunlight on a clear day in September in Champaign, Illinois. The temperature of the TAST-covered skin simulator was measured and compared to that uncovered as bare skin and to that covered with white cotton fabric. As shown in Figure 3a, TAST experienced a temperature drop of 6–10 and 6–14 °C compared to the skin temperatures measured with the cotton-covered and bare skin cases, respectively. Notably, the commercial cotton fabric (0.5 mm) used here was thinner than TAST (1 mm), which could provide better heat convection and conduction. Nevertheless, TAST demonstrated superior cooling performance, underscoring the efficacy of radiative cooling in outdoor conditions.

We also assessed the heating capability of TAST by applying electrical bias to a single fiber thread. For Joule heating, it is highly dependent on the electrical resistance of the metal wire. To obtain sufficiently fast heating with a low voltage, we selected stainless steel as the fiber core material due to its high electrical resistivity ($7.4 \times 10^{-7} \Omega\cdot\text{m}$). Figure 3b depicts the temperature increase rate when different voltages were applied to TAST, with the corresponding current levels provided in Table S1. The data show that even with a small bias of 3–5 V, heating effects of more than 10 °C can be achieved in less than 5 min. Furthermore, TAST can enable localized heating by controlling the bias of the individual fibers. Figure 3c displays the infrared thermal imaging of TAST under different heating modes, i.e., uniform heating and localized heating. The total voltage applied was fixed at 2.5 V. When the voltage was applied to all of the fiber threads, it led to a uniform heating mode. In contrast, selectively biasing only the fibers that traverse the desired regions allows for localized heating.

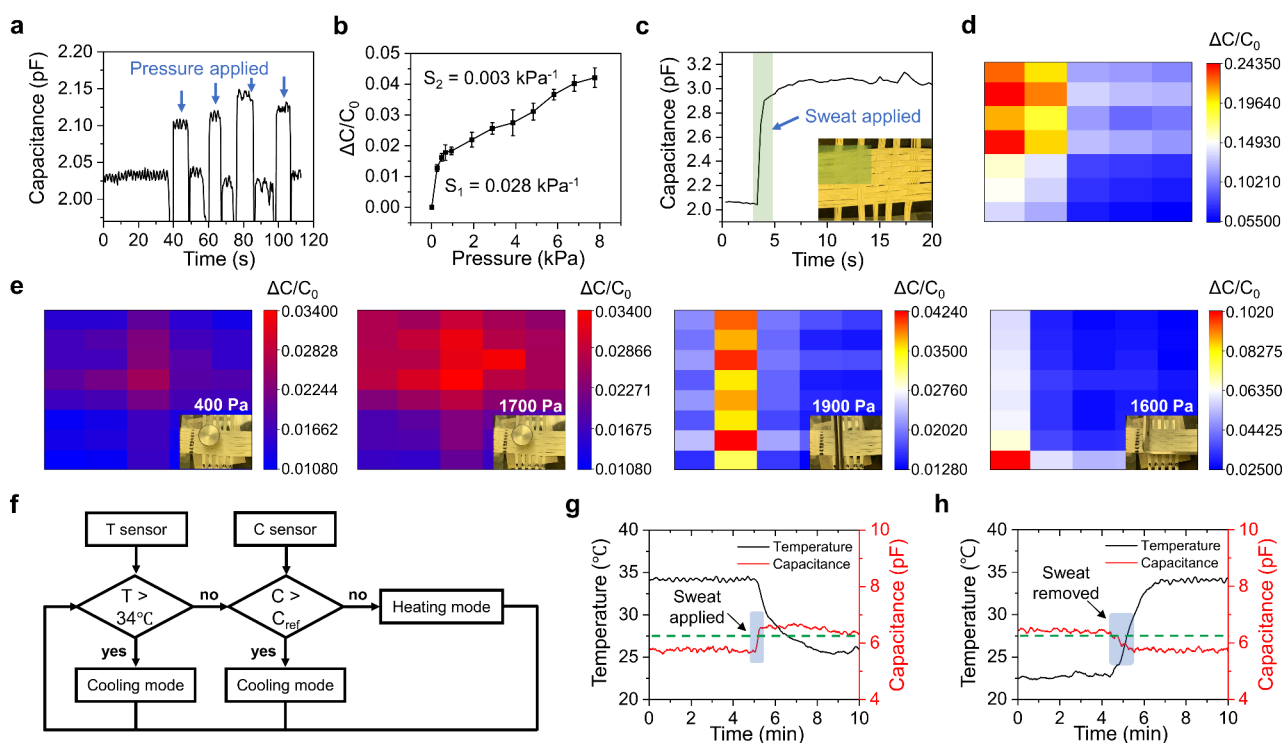


Figure 4. Sensing performance and enhanced smart thermoregulation. (a) Real-time capacitance change of TAST in response to the applied pressure. (b) Relative capacitance change of TAST as a function of pressure. (c) Real-time capacitance change of TAST in response to the presence of sweat. The green shaded region in the inset indicates the location where sweat was applied. Spatial mapping of the relative capacitance changes by the applied (d) sweat and (e) pressures with different intensities and locations. (f) Flow diagram of the closed-loop control system for adaptive thermoregulation controlled by sweat and temperature. Demonstration of the adaptive thermoregulation for TAST with the (g) application and (h) removal of sweat based on the real-time temperature and sweat sensing data from TAST. Green dotted lines indicate a capacitance threshold for mode switching.

Additionally, we confirmed the feasibility of Joule heating in the aforementioned TAST made from carbon fiber cores and PE sheath fibers. Applying voltage to carbon-fiber based TAST could increase the temperature by more than 10 °C within 3 min, as shown in Figures S10 and S11. This confirms that flexible materials such as carbon fibers, possessing suitable electrical conductivity, are appropriate for implementing various heating modes in TAST.

Building on the realization of both cooling and heating functions with TAST, we further demonstrated its adaptive thermoregulation capability by using a closed-loop control system. Figure S12 presents the closed-loop control system diagram for adaptive thermoregulation. This system is designed to maintain the normal skin temperature of the human body at 34–37 °C by dynamically altering the radiative cooling and Joule heating functions. Specifically, when the environment is hot, TAST uses the radiative cooling function to limit the rise in skin temperature, and Joule heating is triggered when the skin temperature falls below 34 °C (Figure 3d). Figure 3e demonstrates the real-time adaptive thermoregulation performance of TAST under varying environmental conditions. The detailed change in ambient temperature is depicted in Figure S13. This temperature changing procedure was performed in multiple cycles to test the reliability of the adaptive thermoregulation function with a closed-loop control system. For comparison, normal cotton fabric was also tested under the same conditions as those in the experimental control group. In a typical indoor environment at the ambient temperature of 22 °C without sunlight, both TAST and cotton can keep the simulated skin at the normal skin temperature of

approximately 34 °C. When exposed to intense direct sunlight in typical outdoor conditions (100 mW/cm²), cotton resulted in a significant rise in skin temperature, reaching up to 45 °C. TAST, on the other hand, provided a radiative cooling effect that resulted in a skin temperature that was 7 °C lower than that for normal cotton, preventing the simulated skin from being overheated beyond the thermal comfort zone. For both the indoor and outdoor cases, as the ambient temperature drastically dropped to ~10 °C (simulated by placing icepacks nearby, illustrated with blue shading in Figure 3e and corresponding ambient temperature data shown in Figure S13), the temperature of the cotton-covered skin simulator was instantly reduced by about 10 °C. In contrast, by activating the Joule heating function, the TAST-covered skin simulator showed minimal temperature decrease and maintained the normal skin temperature of 34 °C. These comparisons demonstrated the effectiveness of TAST in adaptive thermoregulation as a response to environmental changes, which is a desirable capability that is lacking in traditional textiles.

Finally, we evaluated the sensing performance of TAST against sweat and pressure and further utilized the sensing data as feedback signals for precise and autonomous thermoregulation. Each weft and warp thread of the TAST sample used in the sensing tests contained five fibers. When external stimuli, e.g., sweat and pressure, were applied, the capacitance change of an individual sensor unit formed by one weft thread and one warp thread was measured. As shown in Figure 4a, TAST responded in real-time to the applied pressure, with its capacitance increasing as the pressure increased. The pressure sensitivity graph was split into two linear regions (Figure 4b).

In the lower pressure region below 1 kPa, the sensitivity of TAST was measured as 0.0028 kPa^{-1} , and a sensitivity of 0.003 kPa^{-1} was observed in the higher-pressure range of 1 kPa–8 kPa. Figure 4c shows the change in capacitance in response to sweat. When a wet surface simulating the skin with sweat was brought into contact with TAST, the capacitance increased instantly from 2 pF to 3 pF. We should note that the measured capacitance response would not be significantly influenced by humidity in the air, as the change of air permittivity with humidity is relatively small (on the order of $10^{-6}/\%RH$).⁵⁴ Meanwhile, the sweat sensing performance of TAST could be potentially further enhanced by applying moisture-wicking effects, which not only provide additional cooling effects due to faster sweat removal but also result in a larger capacitance change caused by sweat infiltration within the porous layer.⁵⁵ Moreover, because of the weaving structure, TAST contains an array of capacitive sensor units at the cross-points of the warp and weft threads. Thus, TAST also allows for the detection of the stimulus distribution by simultaneously measuring the capacitances of each sensor unit. For example, Figure 4d presents the mapping of the relative capacitance change when sweat was applied on the upper left corner of the TAST sample, based on the raw measurement data shown in Figure S14. It was observed that the relative capacitance changes were higher at the spots that were closer to where sweat was applied, signifying the ability of TAST to identify the spatial distribution of perspiration. Similarly, the spatial distribution of applied pressure can be detected and monitored by integrating the sensing data from each capacitive sensor unit. As shown in Figure 4e and Figure S15, the mapping of the relative capacitance change over TAST can be used to depict a variety of applied pressure scenarios with different intensities and distributions.

As a proof of concept, we integrated the sensing and thermoregulation capabilities of TAST to utilize the monitoring data as control signals for autonomous temperature adjustment. This enables more precise management of thermal comfort based on the physiological status of wearers instead of solely relying on environmental temperatures. For instance, if perspiration develops after engaging in intense physical activities in a cold environment, the body will need cooling rather than heating. To achieve such an advanced intelligent thermoregulation function, a modified diagram of the closed-loop control system was used, as shown in Figure 4f. With the feedback control, TAST can dynamically switch from cooling to heating mode when the following conditions are met: the skin temperature is lower than $34 \text{ }^\circ\text{C}$ and the capacitive sensor detects signals less than the reference value (C_{ref}), indicating no sweating. Conversely, it switches from the heating to cooling mode when the skin temperature is higher than $34 \text{ }^\circ\text{C}$ or the capacitive sensor detects signals exceeding C_{ref} . Figures 4g and 4h demonstrate the performance of TAST in adaptive temperature control in accordance with sweat sensing. When sweat is generated and detected, TAST will deactivate the heating mode and switch to cooling mode to reduce the temperature (Figure 4g). As the sweat evaporates, TAST will change from the cooling to heating mode, raising the temperature to the thermal comfort level (Figure 4h). These results suggest that TAST is capable of intelligent thermoregulation to effectively manage thermal comfort in response to not only temperature variation but also physiological status.

In summary, we created TAST, a woven structured smart textile for intelligent personal thermal management by utilizing

the coaxial extrusion of seamlessly integrated multifunctional core–sheath fibers. TAST is flexible, wearable, breathable, and washable, like other woven fabrics, making it suitable for a wide range of textiles-based applications. More importantly, TAST has the ability to perform radiative cooling, Joule heating, and capacitive sensing functions, which enable adaptive thermoregulation capabilities in response to changes in ambient temperature and detection of perspiration. We believe that TAST will offer a new paradigm for the advancement of smart wearables to track the physiological status of the human body and autonomously adapt their functions to achieve optimal personal thermal management. The coaxial extrusion method presented here can provide a scalable manufacturing platform for further exploration of multifunctional fibers with different components for various wearable technologies.

■ ASSOCIATED CONTENT

Supporting Information

The Supporting Information is available free of charge at <https://pubs.acs.org/doi/10.1021/acsmaterialslett.4c01624>.

Experimental methods; digital photographs, UV–vis and FTIR data, stress strain curve, washability, water contact angle, and infrared thermal image of TAST; schematic diagram of closed-loop control system; adaptive thermoregulation test (PDF)

■ AUTHOR INFORMATION

Corresponding Author

Lili Cai – Department of Mechanical Science and Engineering, University of Illinois at Urbana–Champaign, Urbana, Illinois 61801, United States; Materials Research Laboratory, University of Illinois at Urbana–Champaign, Urbana, Illinois 61801, United States; orcid.org/0000-0003-1222-248X; Email: lilicai@illinois.edu

Authors

Yoon Young Choi – Department of Mechanical Science and Engineering, University of Illinois at Urbana–Champaign, Urbana, Illinois 61801, United States; orcid.org/0000-0001-9524-1621

Kai Zhou – Department of Mechanical Science and Engineering, University of Illinois at Urbana–Champaign, Urbana, Illinois 61801, United States; orcid.org/0000-0003-4653-6436

Ho Kun Woo – Department of Mechanical Science and Engineering, University of Illinois at Urbana–Champaign, Urbana, Illinois 61801, United States; orcid.org/0000-0001-5904-8082

Diya Patel – Department of Mechanical Science and Engineering, University of Illinois at Urbana–Champaign, Urbana, Illinois 61801, United States

Md Salauddin – Department of Mechanical Science and Engineering, University of Illinois at Urbana–Champaign, Urbana, Illinois 61801, United States

Complete contact information is available at:

<https://pubs.acs.org/doi/10.1021/acsmaterialslett.4c01624>

Author Contributions

L.C. conceived and directed the project. Y.Y.C. carried out the experiments for sample fabrication, SEM characterization, UV–vis measurement, thermal imaging measurement and imaging, and sensor measurement. K.Z. contributed to material

synthesis. H.K.W. helped with the FTIR characterization. Y.Y.C. and L.C. wrote the manuscript. D.P. and M.S. assisted in revising the manuscript. All authors discussed the results and commented on the paper. CRediT: **Yoon Young Choi** data curation, formal analysis, investigation, methodology, validation, visualization, writing - original draft; **Kai Zhou** methodology; **HO KUN WOO** data curation, resources, writing - review & editing; **Diya Patel** writing - review & editing; **Md Salauddin** writing - review & editing; **Lili Cai** conceptualization, formal analysis, funding acquisition, supervision, validation, writing - review & editing.

Notes

The authors declare no competing financial interest.

ACKNOWLEDGMENTS

SEM and UV-vis measurements were conducted in the Materials Research Laboratory, University of Illinois. This work was supported by the startup fund from the University of Illinois at Urbana-Champaign and the Office of Naval Research under award number N00014-24-1-2050.

REFERENCES

- (1) Carreras, H.; Zanobetti, A.; Koutrakis, P. Effect of daily temperature range on respiratory health in Argentina and its modification by impaired socio-economic conditions and PM10 exposures. *Environmental pollution* **2015**, *206*, 175–182.
- (2) Sung, T.-I.; Chen, M.-J.; Lin, C.-Y.; Lung, S.-C.; Su, H.-J. Relationship between mean daily ambient temperature range and hospital admissions for schizophrenia: results from a national cohort of psychiatric inpatients. *Science of the total environment* **2011**, *410*, 41–46.
- (3) Lee, J. Y.; Kim, H.; Gasparrini, A.; Armstrong, B.; Bell, M. L.; Sera, F.; Lavigne, E.; Abrutzky, R.; Tong, S.; Coelho, M. d. S. Z. S. Predicted temperature-increase-induced global health burden and its regional variability. *Environ. Int.* **2019**, *131*, No. 105027.
- (4) Vicedo-Cabrera, A. M.; Forsberg, B.; Tobias, A.; Zanobetti, A.; Schwartz, J.; Armstrong, B.; Gasparrini, A. Associations of Inter- and Intraday Temperature Change With Mortality. *Am. J. Epidemiol* **2016**, *183*, 286–293.
- (5) Park, J. E.; Son, W. S.; Ryu, Y.; Choi, S. B.; Kwon, O.; Ahn, I. Effects of temperature, humidity, and diurnal temperature range on influenza incidence in a temperate region. *Influenza Other Respir Viruses* **2020**, *14*, 11–18.
- (6) Luo, H.; Zhu, Y.; Xu, Z.; Hong, Y.; Ghosh, P.; Kaur, S.; Wu, M.; Yang, C.; Qiu, M.; Li, Q. Outdoor Personal Thermal Management with Simultaneous Electricity Generation. *Nano Lett.* **2021**, *21*, 3879–3886.
- (7) Kenny, G. P.; Sigal, R. J.; McGinn, R. Body temperature regulation in diabetes. *Temperature* **2016**, *3*, 119–145.
- (8) Rutkove, S. B.; Veves, A.; Mitsa, T.; Nie, R.; Fogerson, P. M.; Garmirian, L. P.; Nardin, R. A. Impaired Distal Thermoregulation in Diabetes and Diabetic Polyneuropathy. *Diabetes Care* **2009**, *32*, 671–676.
- (9) Yang, M.; He, H.; Du, J.; Peng, H.; Ke, G.; Zhou, Y. Insight into the Kinetic Influence of Oxygen Vacancies on the WO₃ Photoanodes for Solar Water Oxidation. *J. Phys. Chem. Lett.* **2019**, *10*, 6159–6165.
- (10) John Dian, F.; Vahidnia, R.; Rahmati, A. Wearables and the Internet of Things (IoT), Applications, Opportunities, and Challenges: A Survey. *IEEE Access* **2020**, *8*, 69200–69211.
- (11) Kim, J.; Lee, M.; Shim, H. J.; Ghaffari, R.; Cho, H. R.; Son, D.; Jung, Y. H.; Soh, M.; Choi, C.; Jung, S.; et al. Stretchable silicon nanoribbon electronics for skin prosthesis. *Nat. Commun.* **2014**, *5*, 5747.
- (12) Li, J.; Ma, Q.; Chan, A. H.; Man, S. S. Health monitoring through wearable technologies for older adults: Smart wearables acceptance model. *Appl. Ergon* **2019**, *75*, 162–169.
- (13) Wang, L.; Jiang, K.; Shen, G. Wearable, Implantable, and Interventional Medical Devices Based on Smart Electronic Skins. *Advanced Materials Technologies* **2021**, *6*, No. 2100107.
- (14) Indrakumari, R.; Poongodi, T.; Suresh, P.; Balamurugan, B. The growing role of Internet of Things in healthcare wearables. *Emergence of Pharmaceutical Industry Growth with Industrial IoT Approach*; Elsevier, 2020; pp 163–194.
- (15) Chen, M.; Li, P.; Wang, R.; Xiang, Y. Z.; Huang, Z. H.; Yu, Q.; He, M. Y.; Liu, J.; Wang, J. X.; Su, M. Y.; et al. Multifunctional Fiber-Enabled Intelligent Health Agents. *Adv. Mater.* **2022**, *34*, No. 2200985.
- (16) Hong, S.; Gu, Y.; Seo, J. K.; Wang, J.; Liu, P.; Meng, Y. S.; Xu, S.; Chen, R. Wearable thermoelectrics for personalized thermoregulation. *Science advances* **2019**, *5*, No. eaaw0536.
- (17) Lou, L.; Shou, D.; Park, H.; Zhao, D.; Wu, Y. S.; Hui, X.; Yang, R.; Kan, E. C.; Fan, J. Thermoelectric air conditioning undergarment for personal thermal management and HVAC energy saving. *Energy and Buildings* **2020**, *226*, No. 110374.
- (18) Salihoglu, O.; Uzlu, H. B.; Yakar, O.; Aas, S.; Balci, O.; Kakenov, N.; Balci, S.; Olcum, S.; Süzer, S.; Kocabas, C. Graphene-based adaptive thermal camouflage. *Nano Lett.* **2018**, *18*, 4541–4548.
- (19) Sun, Y.; Chang, H.; Hu, J.; Wang, Y.; Weng, Y.; Zhang, C.; Niu, S.; Cao, L.; Chen, Z.; Guo, N. Large-scale multifunctional carbon nanotube thin film as effective mid-infrared radiation modulator with long-term stability. *Advanced Optical Materials* **2021**, *9*, No. 2001216.
- (20) Wang, C.; Dong, H.; Cheng, C.; Sun, K.; Jin, T.; Shi, Q. Flexible and Biocompatible Silk Fiber-Based Composite Phase Change Material for Personal Thermal Management. *ACS Sustainable Chem. Eng.* **2022**, *10*, 16368–16376.
- (21) Peng, Y.; Cui, Y. Advanced textiles for personal thermal management and energy. *Joule* **2020**, *4*, 724–742.
- (22) Ao, X.; Li, B.; Zhao, B.; Hu, M.; Ren, H.; Yang, H.; Liu, J.; Cao, J.; Feng, J.; Yang, Y. Self-adaptive integration of photothermal and radiative cooling for continuous energy harvesting from the sun and outer space. *Proc. Natl. Acad. Sci. U. S. A.* **2022**, *119*, No. e2120557119.
- (23) Zeng, S.; Pian, S.; Su, M.; Wang, Z.; Wu, M.; Liu, X.; Chen, M.; Xiang, Y.; Wu, J.; Zhang, M. Hierarchical-morphology metafabric for scalable passive daytime radiative cooling. *Science* **2021**, *373*, 692–696.
- (24) Cai, L.; Song, A. Y.; Li, W.; Hsu, P. C.; Lin, D.; Catrysse, P. B.; Liu, Y.; Peng, Y.; Chen, J.; Wang, H. Spectrally selective nanocomposite textile for outdoor personal cooling. *Adv. Mater.* **2018**, *30*, No. 1802152.
- (25) Peng, Y.; Chen, J.; Song, A. Y.; Catrysse, P. B.; Hsu, P.-C.; Cai, L.; Liu, B.; Zhu, Y.; Zhou, G.; Wu, D. S. Nanoporous polyethylene microfibrils for large-scale radiative cooling fabric. *Nature sustainability* **2018**, *1*, 105–112.
- (26) Zhu, B.; Li, W.; Zhang, Q.; Li, D.; Liu, X.; Wang, Y.; Xu, N.; Wu, Z.; Li, J.; Li, X. Subambient daytime radiative cooling textile based on nanoprocessed silk. *Nat. Nanotechnol.* **2021**, *16*, 1342–1348.
- (27) Hsu, P.-C.; Song, A. Y.; Catrysse, P. B.; Liu, C.; Peng, Y.; Xie, J.; Fan, S.; Cui, Y. Radiative human body cooling by nanoporous polyethylene textile. *Science* **2016**, *353*, 1019–1023.
- (28) Cai, L.; Peng, Y.; Xu, J.; Zhou, C.; Zhou, C.; Wu, P.; Lin, D.; Fan, S.; Cui, Y. Temperature Regulation in Colored Infrared-Transparent Polyethylene Textiles. *Joule* **2019**, *3*, 1478–1486.
- (29) Cai, L.; Song, A. Y.; Wu, P.; Hsu, P.-C.; Peng, Y.; Chen, J.; Liu, C.; Catrysse, P. B.; Liu, Y.; Yang, A.; Zhou, C.; Zhou, C.; Fan, S.; Cui, Y. Warming up human body by nanoporous metallized polyethylene textile. *Nat. Commun.* **2017**, *8*, 496.
- (30) Woo, H. K.; Zhou, K.; Kim, S. K.; Manjarrez, A.; Hoque, M. J.; Seong, T. Y.; Cai, L. Visibly Transparent and Infrared Reflective Coatings for Personal Thermal Management and Thermal Camouflage. *Adv. Funct. Mater.* **2022**, *32*, No. 2201432.
- (31) Hsu, P. C.; Liu, X.; Liu, C.; Xie, X.; Lee, H. R.; Welch, A. J.; Zhao, T.; Cui, Y. Personal thermal management by metallic nanowire-coated textile. *Nano Lett.* **2015**, *15*, 365–371.

- (32) Dong, X. X.; Cao, Y. M.; Wang, C.; Wu, B.; Zheng, M.; Xue, Y. B.; Li, W.; Han, B.; Zheng, M.; Wang, Z. S.; et al. MXene-Decorated Smart Textiles with the Desired Mid-Infrared Emissivity for Passive Personal Thermal Management. *ACS Appl. Mater. Interfaces* **2023**, *15*, 12032–12040.
- (33) Wang, Y. J.; Wang, T. C.; Liang, J.; Wu, J. W.; Yang, M. P.; Pan, Y. M.; Hou, C.; Liu, C. T.; Shen, C. Y.; Tao, G. M.; et al. Controllable-morphology polymer blend photonic metafoam for radiative cooling. *Mater. Horiz* **2023**, *10*, 5060–5070.
- (34) Wu, J. W.; Zhang, M. N.; Su, M. Y.; Zhang, Y. Q.; Liang, J.; Zeng, S. N.; Chen, B. S.; Cui, L.; Hou, C.; Tao, G. M. Robust and Flexible Multimaterial Aerogel Fabric Toward Outdoor Passive Heating. *Adv. Fiber Mater.* **2022**, *4*, 1545–1555.
- (35) Yin, X.; Yang, R.; Tan, G.; Fan, S. Terrestrial radiative cooling: Using the cold universe as a renewable and sustainable energy source. *Science* **2020**, *370*, 786–791.
- (36) Huang, M. C.; Yang, M. P.; Guo, X. J.; Xue, C. H.; Wang, H. D.; Ma, C. Q.; Bai, Z. X.; Zhou, X. J.; Wang, Z. K.; Liu, B. Y.; et al. Scalable multifunctional radiative cooling materials. *Prog. Mater. Sci.* **2023**, *137*, No. 101144.
- (37) Liang, J.; Wu, J. W.; Guo, J.; Li, H. G.; Zhou, X. J.; Liang, S.; Qiu, C. W.; Tao, G. M. Radiative cooling for passive thermal management towards sustainable carbon neutrality. *Natl. Sci. Rev.* **2023**, *10*, nwac208.
- (38) Zhou, S.; Dong, S.; Guo, Y.; Shuai, Y.; Xu, H.-X.; Hu, G. Colored thermal camouflage and anti-counterfeiting with programmable In₃SbTe₂ platform. *Nanophotonics* **2024**, *13*, 945–954.
- (39) Zhou, S.; Guo, Y.; Zhu, L.; Liu, Y.; Pan, Q.; Shuai, Y.; Hu, G. Continuous Programmable Mid-Infrared Thermal Emitter and Camouflage Based on In₃SbTe₂ Phase-Change Material. *Opt. Lett.* **2023**, *48*, 4388–4391.
- (40) Sui, C.; Pu, J.; Chen, T.-H.; Liang, J.; Lai, Y.-T.; Rao, Y.; Wu, R.; Han, Y.; Wang, K.; Li, X. Dynamic electrochromism for all-season radiative thermoregulation. *Nature Sustainability* **2023**, *6*, 428–437.
- (41) Rao, Y.; Dai, J.; Sui, C.; Lai, Y.-T.; Li, Z.; Fang, H.; Li, X.; Li, W.; Hsu, P.-C. Ultra-wideband transparent conductive electrode for electrochromic synergistic solar and radiative heat management. *ACS Energy Letters* **2021**, *6*, 3906–3915.
- (42) Mandal, J.; Jia, M.; Overvig, A.; Fu, Y.; Che, E.; Yu, N.; Yang, Y. Porous polymers with switchable optical transmittance for optical and thermal regulation. *Joule* **2019**, *3*, 3088–3099.
- (43) Fei, J.; Han, D.; Ge, J.; Wang, X.; Koh, S. W.; Gao, S.; Sun, Z.; Wan, M. P.; Ng, B. F.; Cai, L. Switchable surface coating for bifunctional passive radiative cooling and solar heating. *Adv. Funct. Mater.* **2022**, *32*, No. 2203582.
- (44) Bohren, C. F.; Huffman, D. R. *Absorption and scattering of light by small particles*; John Wiley & Sons, 2008.
- (45) Zhao, Q.; Zhou, J.; Zhang, F.; Lippens, D. Mie resonance-based dielectric metamaterials. *Mater. Today* **2009**, *12*, 60–69.
- (46) Evlyukhin, A. B.; Reinhardt, C.; Seidel, A.; Luk'yanchuk, B. S.; Chichkov, B. N. Optical response features of Si-nanoparticle arrays. *Phys. Rev. B* **2010**, *82*, No. 045404.
- (47) Xue, C.-H.; Wei, R.-X.; Guo, X.-J.; Liu, B.-Y.; Du, M.-M.; Huang, M.-C.; Li, H.-G.; Jia, S.-T. Fabrication of superhydrophobic P(VDF-HFP)/SiO₂ composite film for stable radiative cooling. *Compos. Sci. Technol.* **2022**, *220*, No. 109279.
- (48) Cheng, Z.; Shuai, Y.; Gong, D.; Wang, F.; Liang, H.; Li, G. Optical properties and cooling performance analyses of single-layer radiative cooling coating with mixture of TiO₂ particles and SiO₂ particles. *Science China Technological Sciences* **2021**, *64*, 1017–1029.
- (49) Son, S.; Lee, T. Y.; Chae, D.; Lim, H.; Ha, J.; Kim, Y. K.; Lee, H. Efficient Daytime Radiative Cooling Cover Sheet with Dual-Modal Optical Properties. *Advanced Optical Materials* **2022**, *10*, No. 2201771.
- (50) Zhou, K.; Li, W.; Patel, B. B.; Tao, R.; Chang, Y.; Fan, S.; Diao, Y.; Cai, L. Three-Dimensional Printable Nanoporous Polymer Matrix Composites for Daytime Radiative Cooling. *Nano Lett.* **2021**, *21*, 1493–1499.
- (51) Lloyd, D. R.; Kinzer, K. E.; Tseng, H. Microporous membrane formation via thermally induced phase separation. I. Solid-liquid phase separation. *J. Membr. Sci.* **1990**, *52*, 239–261.
- (52) Bansil, R. Phase separation in polymer solutions and gels. *Le Journal de Physique IV* **1993**, *3*, C1-225–C221-235.
- (53) Tong, J. K.; Huang, X.; Boriskina, S. V.; Loomis, J.; Xu, Y.; Chen, G. Infrared-transparent visible-opaque fabrics for wearable personal thermal management. *ACS Photonics* **2015**, *2*, 769–778.
- (54) Zarnik, M. S.; Belavic, D. An Experimental and Numerical Study of the Humidity Effect on the Stability of a Capacitive Ceramic Pressure Sensor. *Radioengineering* **2012**, *21*, 201–206.
- (55) Zhang, X.; Yang, W.; Shao, Z.; Li, Y.; Su, Y.; Zhang, Q.; Hou, C.; Wang, H. A moisture-wicking passive radiative cooling hierarchical metafabric. *ACS Nano* **2022**, *16*, 2188–2197.